IOP Publishing Nanotechnology
Nanotechnology 28 (2017) 365501 (8pp) https://doi.org/10.1088/1361-6528/aa7d66

Molybdenum disulfide nanoparticles decorated reduced graphene oxide: highly sensitive and selective hydrogen sensor

A Venkatesan[1], Servin Rathi[2], In-yeal Lee[2], Jinwoo Park[2], Dongsuk Lim[2], Moonshik Kang[2], Han-Ik Joh[3,4], Gil-Ho Kim[2,5] and E S Kannan[1,5]

[1] Department of Physics, BITS-Pilani, K. K. Birla Goa Campus, Zuarinagar, Goa 403726, India
[2] School of Electronic and Electrical Engineering and Sungkyunkwan Advanced Institute of Nanotechnology (SAINT), Sungkyunkwan University, Suwon 16419, Republic of Korea
[3] Carbon Convergence Materials Research Center, Institute of Advanced Composite Materials, Korea Institute of Science and Technology, Jeollabuk-do, 55324, Republic of Korea
[4] Department of Energy Engineering, Konkuk University, 120 Neungdong-ro, Gwangjin-gu, Seoul 05029, Republic of Korea

E-mail: ghkim@skku.edu and eskannan@goa.bits-pilani.ac.in

Received 25 April 2017, revised 28 June 2017
Accepted for publication 4 July 2017
Published 14 August 2017

Abstract

In this work, we report on the hydrogen (H_2) sensing behavior of reduced graphene oxide (RGO)/molybdenum disulfide (MoS_2) nano particles (NPs) based composite film. The RGO/MoS_2 composite exhibited a highly enhanced H_2 response (~15.6%) for 200 ppm at an operating temperature of 60 °C. Furthermore, the RGO/MoS_2 composite showed excellent selectivity to H_2 with respect to ammonia (NH_3) and nitric oxide (NO) which are highly reactive gas species. The composite's response to H_2 is 2.9 times higher than that of NH_3 whereas for NO it is 3.5. This highly improved H_2 sensing response and selectivity of RGO/MoS_2 at low operating temperatures were attributed to the structural integration of MoS_2 nanoparticles in the nanochannels and pores in the RGO layer.

Supplementary material for this article is available online

Keywords: graphene oxide, composite, gas sensor, thin film

(Some figures may appear in colour only in the online journal)

1. Introduction

Detection of hydrogen (H_2) is more important and critical as its usage has become more ubiquitous in many fields such as agriculture, public health, transportation and industries [1, 2]. Energy from hydrogen is one of the promising alternatives to fossil fuels and it demands development of highly sensitive, low cost, and portable gas sensors with low power consumption [3]. Solid state gas sensors based on nanostructures like carbon nanotubes, 1D semiconducting wires and 2D graphene sheets have shown great promise in sensing applications [4, 5]. However, all these sensors require higher temperature for their operation resulting in more energy consumption. Recently, 2D transition metal dichalcogenides (TMDCs) based nanomaterials have attracted immense attention because they are found to exhibit wide range of physical and chemical properties. Most of the TMDC materials such as molybdenum disulfide (MoS_2), tungsten selenide, molybdenum selenide, tungsten disulfide and black phosphorus have tunable band gap, highly reactive surfaces, good optical absorption and high mechanical strength [6–11]. Of all the TMDC materials, nanostructured MoS_2 is a very promising candidate for gas sensors as it has high density of surface active sites [12].

In spite of having excellent surface properties, there are only few reports on its potential as a viable and effective

[5] Authors to whom any correspondence should be addressed.

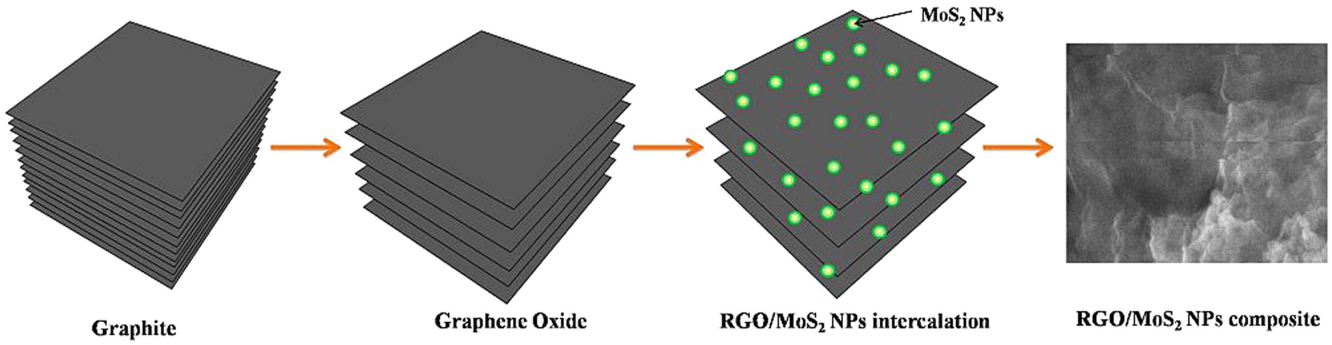

Figure 1. Schematic representation of formation of RGO/MoS_2 composite sensing layer. (a) Graphite (b) graphene oxide (GO) preparation by modified hummer's method (c) RGO/MoS_2 composite (d) FE-SEM image of RGO/MoS_2 composite.

chemical and gas sensor. The main bottleneck in using MoS_2 in sensing application is the stacking arrangement of Mo and S layer. It is a lamellar compound, consisting of three atomic layers which are held together by weak van der waals interaction: Mo layer sandwiched between two S layers. This van der waals interaction inevitably results in aggregation phenomenon which decreases the number of active sites as well as the whole sensing activity [13]. If MoS_2 based nanomaterials are to realize their potential, then there is an urgent need to increase the number of active sites. One method is to functionalize or hybridize this material with conductive templates or supports such as graphene or graphene oxide whose structural stability prevents the aggregation of MoS_2 nanoparticles [14]. Taking these factors into account, we have hybridized MoS_2 nanoparticles with reduced graphene oxide (RGO) to improve the sensing characteristics.

In this work, we embedded MoS_2 nanoparticles into RGO matrix producing size controlled MoS_2/RGO composites for gas sensing. Here the RGO plays the dual role of support matrix for MoS_2 nanoparticles for better mechanical stability and also as a catalyst for enhancing their gas sensing response. We have shown through this work that MoS_2 integrated with RGO have excellent sensing response and selectivity to H_2 at temperatures as low as 40 °C. We hope that our work could help to accelerate RGO/MoS_2 based composites in hydrogen sensing applications and provide more possibilities for future development.

2. Materials and methods

2.1. Synthesis of graphene oxide

Graphene oxide (GO) was synthesized by modified Hummer's method [15, 16]. Prior to drop casting process, the concentration of as prepared GO solution was diluted to 25% by the addition of pure DI water. Then it was ultra sonicated for 45 min to reduce the size of GO flakes and then centrifuged at 15 000 rpm for 5 min in order to remove the thicker flakes. The top portion of the solution was collected in a vial and stored in room temperature for the further use.

2.2. Synthesis of molybdenum disulfide (MoS_2) nanoparticles

In a typical synthesis procedure, 0.3 g of ammonium tetrathiomolybdate ($(NH_4)_2MoS_4$ (0.3 g) was dissolved in 100 ml of DI water for 30 min. During the dissolving procedure, 2 ml of hydrochloric acid (HCl) was added to the above solution and for sufficient reaction 30 min ultrasonication was provided. This resulted in a change in color of the solution from red to black indicating the formation of MoS_2 nanoparticles. Finally the end product was vacuum filtered and washed with copious amount of DI water and dried at 60 °C in convection air oven for 12 h.

2.3. Fabrication of gas sensor

The electrodes for the sensors were fabricated on silicon (Si) substrate with 300 nm SiO_2 layer. Before the fabrication, the silicon substrates were cleaned in acetone, ethanol and deionized water by ultrasonication followed by drying in nitrogen flow. The interdigitated electrodes were fabricated by e-beam evaporation by depositing 10 nm Ti and 100 nm Au onto a lithographically patterned photoresist.

After the metal deposition, photoresist were removed by lift-off process. The resultant electrodes were washed with ethanol and copious amount of deionized water and finally dried by nitrogen flow. For sensing layer preparation, 1 mg of MoS_2 nanoparticles in powder form was added to 0.5 ml of organic GO solution and ultrasonicated for 1 h to produce uniform dispersion. 3 μl of solution containing the above dispersion was drop casted on the metal electrodes and annealed at 400 °C (figures 1(a)–(d)). For comparison, a control sample was prepared using pure GO solution with the same experimental condition as mentioned above.

2.4. Hydrogen gas sensing technique

The gas sensing measurements were carried out in a closed chamber equipped with PID controlled electrical heater. Before starting the sensing measurement, the chamber was evacuated to $\sim 2 \times 10^{-5}$ mbar by rotary pump. The sensing measurement was performed by sending high purity H_2, NO, and NH_3 gases to the gas sensing chamber. The flow rate was controlled using mass flow controllers and sensing response of the composite was monitored by measuring the change in current [17].

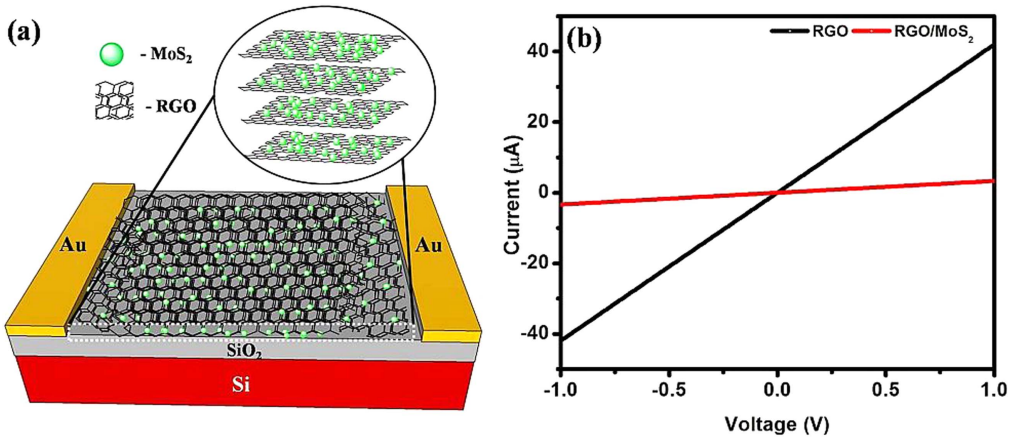

Figure 2. (a) Schematic illustration of RGO/MoS_2 sensing device. (b) *I–V* characteristics of RGO/MoS_2 based device.

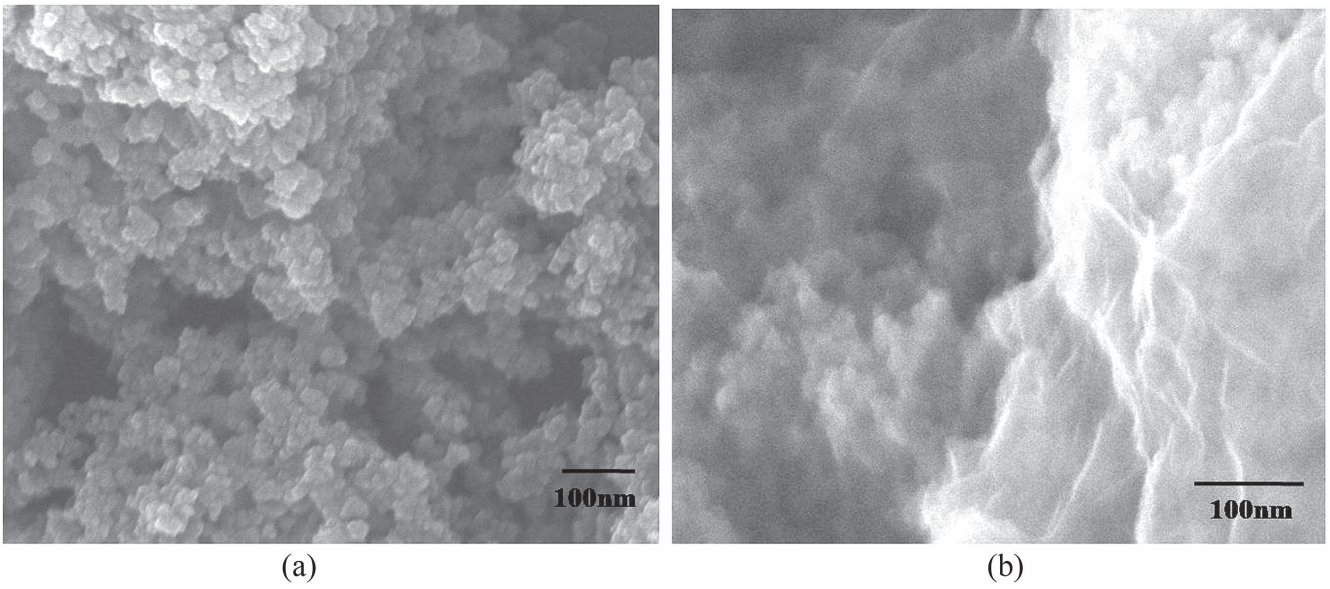

Figure 3. FE-SEM image of as prepared (a) MoS_2 nanoparticles and (b) RGO/MoS_2 NPs composite.

3. Results and discussions

Figure 2(a) shows the schematic diagram of RGO/MoS_2 and RGO based hydrogen sensor. Room temperature current–voltage (*I–V*) characteristics (figure 2(b)) exhibited linear behavior with the RGO/MoS_2 (28 MΩ) composite showing 10 times more resistance than pure RGO (2.3 MΩ). This can be explained by the fact that the incorporated MoS_2 nanoparticles result in a hole depletion region of the RGO layer near the interface with n-type MoS_2 nanoparticles [18, 19].

Figures 3(a) and (b) shows the surface morphology of pure MoS_2 and RGO/MoS_2 composite. The as prepared MoS_2 nanoparticles (size ∼ 32 nm) after dispersion onto a silicon substrate instantaneously agglomerated as their surfaces have high density of active sites (figure 3(a)). Upon dispersing MoS_2 nanoparticles into RGO, they are found to be homogenously dispersed as shown in figure 3(b). This clearly shows that the RGO is an ideal matrix material for MoS_2 nanoparticles to retain their surface properties. Furthermore, the RGO/MoS_2 was also characterized by AFM and TEM techniques (see supplementary S3 and S4 is available online at stacks.iop.org/NANO/28/365501/mmedia). From the AFM images, the thickness of active device channel was found to be ∼15 nm.

The atomic valence states and the composition of the MoS_2/RGO composites were characterized by x-ray photoelectron spectroscopy (XPS) and the following elements were identified: C, O, Mo, and S. In the C 1s XPS spectrum of GO, the three observable peaks correspond to C=O (288.3 eV), C–O (286.7 eV), and C–C (284.5 eV) groups respectively (figure 4(a)). For RGO/MoS_2 composite the intensities of all C 1s peaks pertaining to functional groups C=O, C–O, and C–C has decreased to a large extent (figure 4(b)). This is a confirmation of effective removal of oxygen functional groups after the annealing treatment. Figure 4(c) shows high resolution XPS spectrum of RGO/MoS_2 composite in the Mo3d region. It can be deconvoluted into four peaks; the two intense peaks observed at 229.6 and 232.8 eV are characteristics signature of Mo 3d5/2 and Mo 3d3/2 states respectively. The peak observed at 226.8 eV corresponds to S 2s

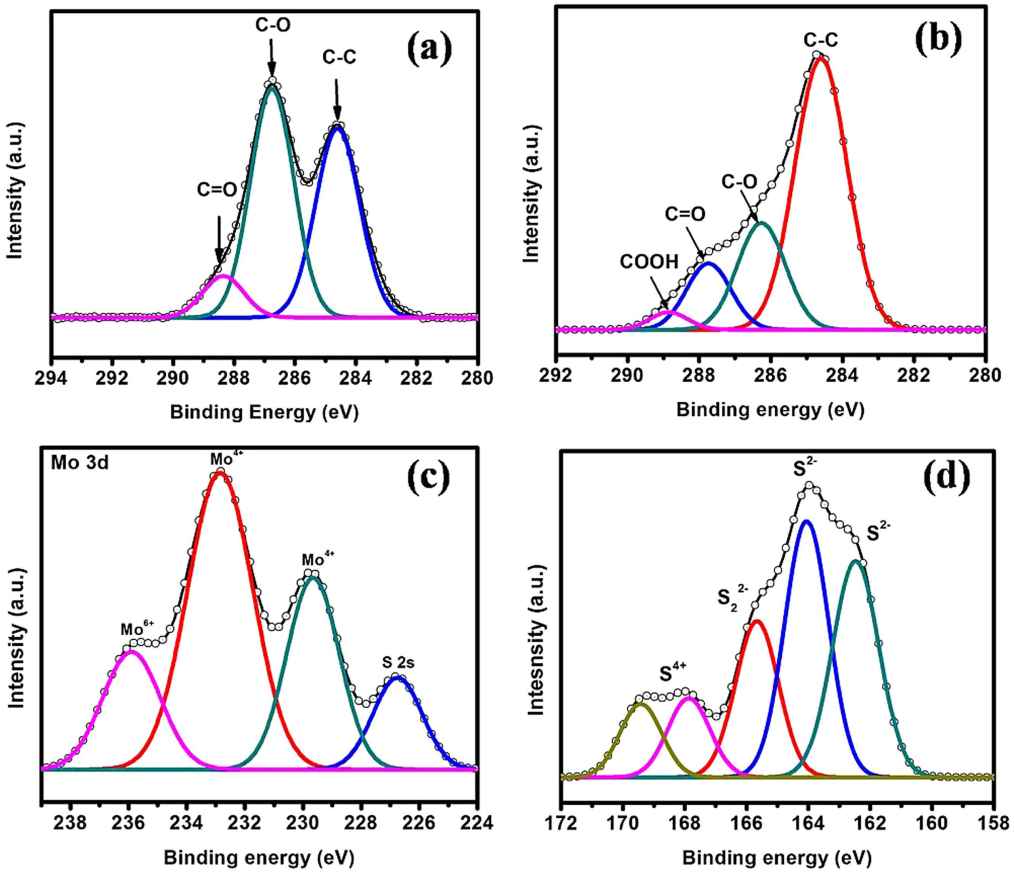

Figure 4. (a) C1s XPS spectrum of GO (b) C1s spectrum of RGO/MoS_2 nanoparticles composite (c) Mo3d spectrum of RGO/MoS_2 and (d) S 2p spectra of RGO/MoS_2 NPs composite.

state of MoS_2, while the high binding energy peak observed at 236 eV can be attributed to Mo3d state of MoO_3 or MoO_4^{2-}, which may result from the oxidation of the composite sample in air. Furthermore, S 2p spectra of RGO/MoS_2 exhibited two main doublets located at binding energies of 162.4 and 164.0 eV corresponds to S $2p_{3/2}$ and S $2p_{1/2}$ lines of MoS_2 (figure 4(d)). Additionally, the binding energy at 165.6 eV suggests the existence of bridging disulfides S_2^{2-} and S^{2-}. The high energy peak observed at 167.8 eV can be assigned to S^{4+} species in sulfate groups (SO_3^{2-}) which are usually observed at the edges of MoS_2 nanoparticles [14, 17].

3.1. Gas sensing properties

The gas sensing response of RGO/MoS_2 was assessed by monitoring the resistance change upon exposure to trace concentrations (200 and 500 ppm) of H_2, NO and NH_3 at operating temperatures ranging from RT to 60 °C. It was monitored with semiconductor characterization system (Keithley 4200 SCS) at different operating temperature. 1 V was applied to sensing device and response towards H_2 was calculated according the following equation [20].

$$R(\%) = 100 \times \Delta R/R_o = 100 \times (R_{gas} - R_o)/R_o, \quad (1)$$

where R_o is the resistance of RGO/MoS_2 device before the exposure to H_2 gas, and R_{gas} is the resistance of the device in the presence of H_2. Hydrogen was introduced (400 s) and removed (300 s) from the gas chamber periodically. Both introduction and removal of H_2 was considered as a single period (700 s). H_2 concentration was fixed at 200 ppm for the first period and at the end of the cycle, the concentration was increased to 500 ppm. This results in a sensing curve containing two periods in series for a particular operating temperature as shown in figure 5. For comparison, pure RGO, prepared by using the same experimental condition, is used as a control sample. Figure 5 shows the typical H_2 sensing profiles of RGO and RGO/MoS_2 with the concentrations of 200 and 500 ppm at different operating temperatures (RT, 40 °C and 60 °C). For the RGO/MoS_2 sensor, the sensing response was very sharp with resistance increasing rapidly as H_2 gas is introduced. It also showed reasonably quick recovery after removing the H_2 gas. Considering the fact that only 200 ppm of H_2 gas was used, the sample seemed to possess remarkable sensing response to H_2 gas. Control sample RGO showed similar characteristics but with significantly lower responsivity.

For RGO/MoS_2, at room temperature, the response plateaued at ~1.1% for 200 ppm of H_2 and across all concentrations ranges. The response however significantly increased to 15.6% on heating the sample to 60 °C. From the sensing response of the control sample and composite, it is quite evident that addition of MoS_2 nanoparticles had improved the responsivity by 81%. The response of control

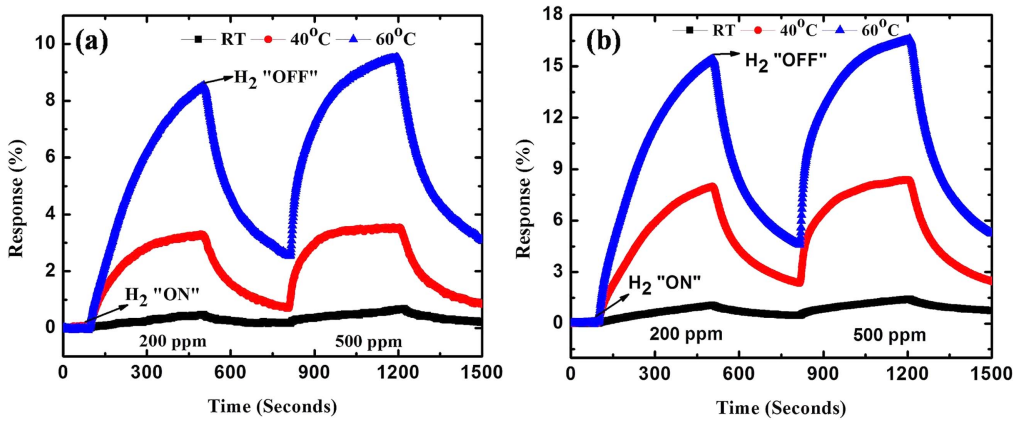

Figure 5. Hydrogen sensing response of (a) RGO and (b) RGO/MoS_2 composite at operating temperatures of RT, 40 °C and 60 °C for the concentration of 200–1000 ppm.

Table 1. Comparison of H_2 sensing response of the RGO/MoS_2 nanoparticles composite prepared in this work with those reported in the literature.

Materials	Working temperature (°C)	Concentration (ppm)	Response (%)	(Year)
Reduced graphene oxide/ZnO nanocomposite	150 °C	200	3.5	2014 [23]
Pd–Pt nanoparticles-reduced graphene oxide composite	40	20 000	5	2011 [24]
Ni–Pd/graphene oxide composite	RT	1000	4	2014 [25]
Reduced oxide and TiO_2	85 °C	5000	1.02	2014 [26]
Reduced graphene oxide and SnO_2 composite	RT	10 000	1.5	2012 [27]
Pd doped reduced graphene oxide	50 °C	3300	~11	2013 [28]
RGO–MoS_2 nanoparticles	60 °C	200	15.6	This work

sample and composite seemed to vary very little with increase in H_2 concentration. This is due to the fact that the sensing response depends mainly on the active surface area of the sensing materials. RGO with its planar structure offers maximum exposure to active sites for H_2 and hence exhibits good sensitivity even for lower gas concentration. In the case of composite the presence of MoS_2 nanoparticles improved the sensing response by providing more active sites for H_2 bonding.

Table 1 shows the sensing characteristics of various RGO based solid state H_2 sensors. From the table it is clear that RGO/MoS_2 based H_2 sensor exhibits better sensing response at 60 °C compared to other solid state sensors which required either higher operating temperature or higher concentration of H_2 to show similar response. On the other hand, in this work we have shown that the RGO/MoS_2 could show sensing response of 15.6% for the same amount of H_2 at the operating temperature of 60 °C. This further confirms that RGO/MoS_2 composite can be a suitable material for sensing low concentration of H_2 at relatively low operating temperature.

The response and recovery time of RGO/MoS_2 composite for 200 ppm of H_2 were found to be 251 and 260 s respectively. Considering the fact that this parameter is obtained for an operating temperature of 60 °C, the sensing characteristics of this composite scales relatively higher than other solid state H_2 sensors [21, 22].

For practical sensing applications, a sensor should be highly selective to various gases. Therefore, we investigated the selectivity of RGO/MoS_2 sensors by exposing NO and NH_3 for different concentration (200–500 ppm) at different operating temperatures (RT, 40 °C and 60 °C). Selectivity is quantified by taking the ratio of sensing response of H_2 with respect to other gases such as NO and NH_3 which are used in this study. The selectivity ratio or selectivity coefficient (K_{SC}) of H_2 for other gases such as NO and NH_3 were calculated using the following equation [29].

$$K_{SC} = \frac{S_{H_2}}{S_{NO,NH_3}}, \quad (2)$$

where S_{H_2}, S_{NO} and S_{NH_3} are the responses of the sensor to H_2, NO and NH_3 gases respectively.

Table 2. The selectivity coefficient 'K_{SC}' of the RGO–MoS_2 nanoparticles based H_2 sensor at 200 ppm in comparison to ammonia (NH_3) and nitric oxide (NO) gases at different operating temperature.

	K_{SC} at 200 ppm		
Operating temperature	RT	40 °C	60 °C
Ammonia	1.05	2.5	2.9
Nitric oxide	1.3	2.9	3.6

Table 2 lists the selectivity coefficient 'K_{SC}' of RGO/MoS_2 based H_2 sensor for 200 ppm operated at RT, 40 °C and 60 °C. The selectivity coefficient 'K_{SC}' for the operating temperature 60 °C is the highest. The higher values of K_{SC} indicates the more selective detection of H_2, that is the value of $K_{SC} = 3.6$ for NO suggests that the H_2 response of

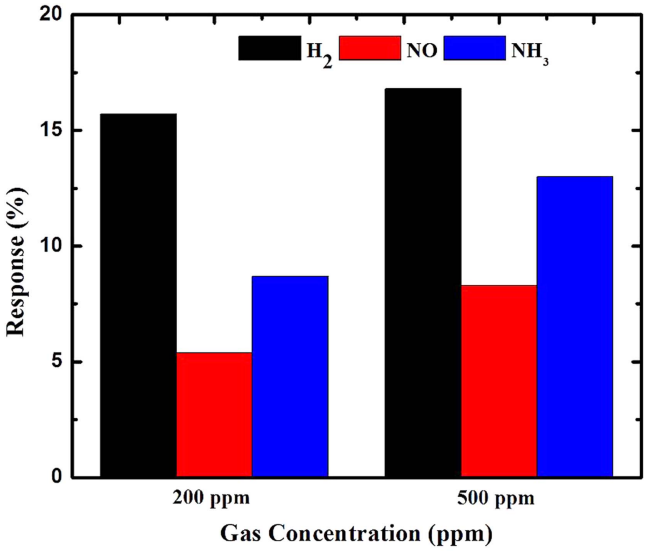

Figure 6. Comparative sensing response of RGO/MoS_2 nanoparticles based composite at 60 °C for 200 and 500 ppm concentrations of H_2, NO and NH_3.

RGO/MOS_2 is 3.6 higher than that of NO whereas $K_{SC} = 2.9$ for NH_3 shows that H_2 response is 2.9 times higher. It is to be pointed out that both NH_3 and NO are highly reactive gases due to the presence of unpaired electrons which allows them to easily bond with any surface. Greater selectivity shown by the composite to H_2 can only be related to the size effect. H_2 being very small in comparison to NO and NH_3 can percolate through defects and pores and access the active sites present underneath the surface [30, 31]. This leads to higher response for H_2 in comparison to other gases. Figure 6 shows the comparison of selective H_2 response of RGO/MoS_2 layer compared to NO and NH_3 at different concentrations at 60 °C.

It is also to be noted that, the addition of MoS_2 nanoparticles also improved the sensing response characteristics of RGO towards NH_3 and NO as in the case of H_2 (figure S1 supplementary information). However, the improvement was more significant for H_2 in comparison to NO and NH_3, which can be attributed to the structural characteristics of sensing layer. From the FE-SEM images, it can be clearly seen that MoS_2 nanoparticles are incorporated into RGO layer such that some nanoparticles are anchored on the top surface of RGO layer and some are underneath it. These structures play a significant role in sensing characteristics of the composite. Recently, it has been reported that graphene oxide is tortuous in nature with the presence of nanochannels in the space between each graphene oxide layers [32, 33]. The pores in the graphene oxide acts as the permeation route for gases with very small size. When the sensing gases (H_2, NH_3, and NO) is exposed to RGO/MoS_2 layer the gases have the possibility of interacting with (i) RGO layer, (ii) MoS_2 nanoparticles anchored on RGO and (iii) MoS_2 nanoparticles which are present underneath the RGO layer. The highly improved H_2 sensing response characteristics of RGO/MoS_2 compared to other (NH_3 and NO) gases can be attributed to interaction of H_2 gas with MoS_2 nanoparticles anchored on the top and bottom surface of RGO. The top RGO layers serves as a filtering layer which selectively permits only H_2 gas due to its smaller size to pass through and interact with MoS_2 nanoparticles buried underneath. However, for both NH_3 and NO percolation is not possible due to their larger sizes and their activity is confined to the top surface. Figure 7 depicts the sensing mechanism involved in RGO/MoS_2. H_2 molecule with their smaller size were able to easily permeate through the nanochannels/nanopores (red circles) and defects whereas this permeation is very limited for NH_3 and NO because of their huge sizes. This phenomenon can be attributed to the improved sensing response characteristics of RGO/MoS_2 for H_2 over NH_3 and NO.

3.2. Sensing mechanism

The sensing mechanism (resistance change on exposure to H_2) of RGO/MoS_2 can be explained based on the interaction between hydrogen atom and chemisorbed oxygen ions (O_2^-) on the surfaces or at the interfaces (heterojunction) of the RGO/MoS_2 nanocomposite. The adsorption of oxygen molecules on the surface of MoS_2 or RGO/MoS_2 interface can be given by [30],

$$O_2 + e^- \rightarrow O_2^-.$$

Upon injection of hydrogen the net reaction can be given by,

$$2H_2 + O_2^- \rightarrow H_2O + e^-.$$

A space charge layer is formed on the surface of MoS_2 nanoparticles when the electrons are trapped by the adsorbed oxygen species forming a high resistance state. When H_2 is introduced, the H_2 molecules react with the ionic oxygen species, and the electrons trapped by the oxygen adsorbents are then released back to MoS_2 nanoparticles, forming a low resistance state. In addition, the Schottky barrier around the interface of RGO and MoS_2 can result in the specific capture and migration of electrons from MoS_2 nanoparticles to RGO nanosheets. Thus the role of RGO nanosheets as an electron mediator further facilitates the transfer of electrons from H_2 molecules to the RGO/MoS_2 nanostructure (figure 8). All the above reasons make the conductivity undergo greater changes and improve the gas sensing performance of the RGO/MoS_2 composite.

4. Conclusions

Highly sensitive and selective RGO/MoS_2 based H_2 sensor was fabricated by facile drop coating technique. The as prepared RGO/MoS_2 sensor exhibited an 81% improvement in the sensing response for the concentration of 200 ppm at the operating temperature of 60 °C compared to pure RGO sensor. In addition, this RGO/MoS_2 based sensor was found to be highly selective towards H_2 compared to NH_3 and NO with selective coefficient (K_{SC}) of 2.9 and 3.5. We envisage that the RGO/MoS_2 nanoparticles based composite can be a potential candidate for H_2 sensing device applications at low operating temperature.

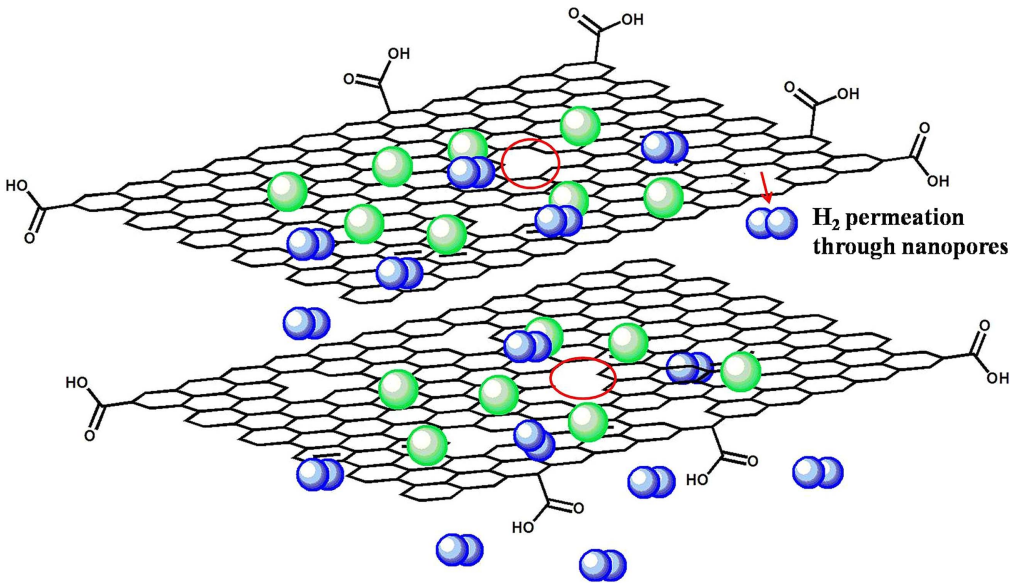

Figure 7. (a) Schematic representation of type III interaction of H_2 sensing in RGO/MoS_2 nanoparticles based composite.

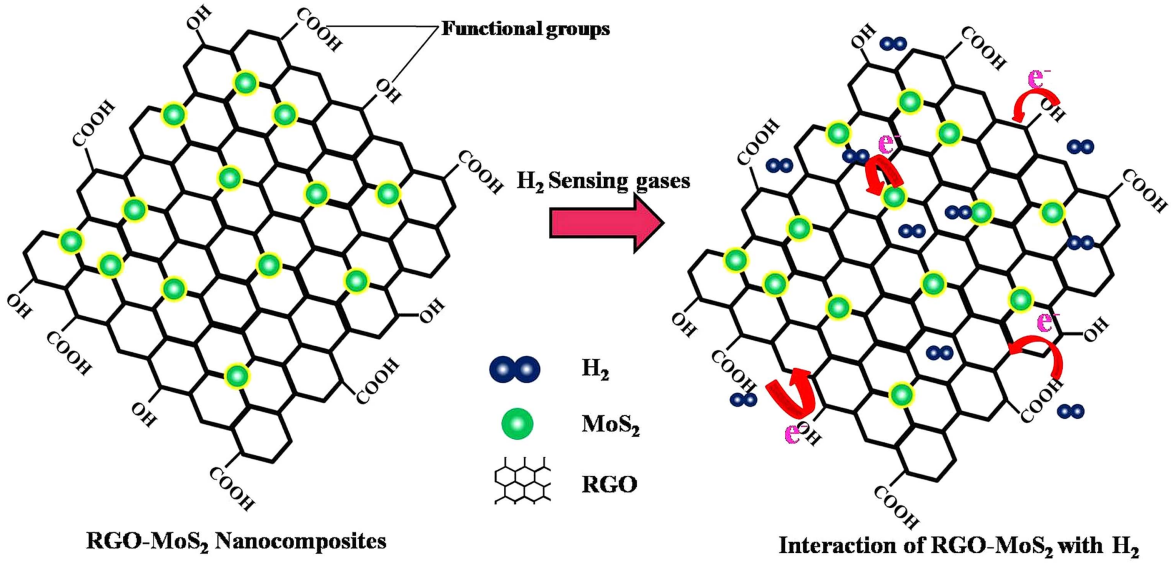

Figure 8. Schematic representation of H_2 sensing mechanism of RGO/MoS_2 nanoparticles based composite.

Acknowledgments

This work was supported by Science and Engineering Research Board under Individual Centric Extra Mural Research Funding (EMR/2016/002628) and Basic Science Research Program through the National Research Foundation of Korea (NRF) funded by the Ministry of Education, Science and Technology (2016R1A2A2A05921925 and 2016R1D1A1B03932455) and Korea Research Fellowship Program through the NRF funded by the Ministry of Science, ICT and Future Planning (2015H1D3A1062519). A Venkatesan would like to acknowledge the financial support from BITS, Pilani—K K Birla Goa Campus, India.

References

[1] Hu Y *et al* 2016 Rapid response hydrogen sensor based on nanoporous Pd thin films *Int. J. Hydrog. Energy* **41** 10986–90
[2] Hübert T, Boon-Brett L, Black G and Banach U 2011 Hydrogen sensors—a review *Sensors Actuators* B **157** 329–52
[3] Hassan J J, Mahdi M A, Chin C W, Abu-Hassan H and Hassan Z 2013 A high-sensitivity room-temperature hydrogen gas sensor based on oblique and vertical ZnO nanorod arrays *Sensors Actuators* B **176** 360–7
[4] Jennifer S-O *et al* 2005 Carbon nanotube films for room temperature hydrogen sensing *Nanotechnology* **16** 2218
[5] Russo P A *et al* 2012 Room-temperature hydrogen sensing with heteronanostructures based on reduced graphene oxide and tin oxide *Angew. Chem., Int. Ed.* **51** 11053–7

[6] Li H *et al* 2012 Fabrication of single- and multilayer MoS_2 film-based field-effect transistors for sensing NO at room temperature *Small.* **8** 63–7

[7] Erande M B, Pawar M S and Late D J 2016 Humidity sensing and photodetection behavior of electrochemically exfoliated atomically thin-layered black phosphorus nanosheets *ACS Appl. Mater. Interfaces* **8** 11548–56

[8] Pawbake A S, Waykar R G, Late D J and Jadkar S R 2016 Highly transparent wafer-scale synthesis of crystalline WS_2 nanoparticle thin film for photodetector and humidity-sensing applications *ACS Appl. Mater. Interfaces* **8** 3359–65

[9] Late D J, Doneux T and Bougouma M 2014 Single-layer $MoSe_2$ based NH_3 gas sensor *Appl. Phys. Lett.* **105** 233103

[10] Late D J *et al* 2013 Sensing behavior of atomically thin-layered MoS_2 transistors *ACS Nano.* **7** 4879–91

[11] Late D J 2016 Liquid exfoliation of black phosphorus nanosheets and its application as humidity sensor *Microporous Mesoporous Mater.* **225** 494–503

[12] Kannan P K, Late D J, Morgan H and Rout C S 2015 Recent developments in 2D layered inorganic nanomaterials for sensing *Nanoscale* **7** 13293–312

[13] Li F *et al* 2015 Synthesis of Cu–MoS_2/rGO hybrid as non-noble metal electrocatalysts for the hydrogen evolution reaction *J. Power Sources* **292** 15–22

[14] Zheng X, Xu J, Yan K, Wang H, Wang Z and Yang S 2014 Space-confined growth of MoS_2 nanosheets within graphite: the layered hybrid of MoS_2 and graphene as an active catalyst for hydrogen evolution reaction *Chem. Mater.* **26** 2344–53

[15] Hirata M, Gotou T, Horiuchi S, Fujiwara M and Ohba M 2004 Thin-film particles of graphite oxide: I. High-yield synthesis and flexibility of the particles *Carbon* **42** 2929–37

[16] Venkatesan A *et al* 2016 Low temperature hydrogen sensing using reduced graphene oxide and tin oxide nanoflowers based hybrid structure *Semicond. Sci. Technol.* **31** 125014

[17] Liu Y, Zhao Y, Jiao L and Chen J 2014 A graphene-like MoS_2/graphene nanocomposite as a highperformance anode for lithium ion batteries *J. Mater. Chem.* A **2** 13109–15

[18] Ahmed F, Choi M S, Liu X and Yoo W J 2015 Carrier transport at the metal–MoS_2 interface *Nanoscale* **7** 9222–8

[19] Mishra R K *et al* 2015 SnO_2 quantum dots decorated on RGO: a superior sensitive, selective and reproducible performance for a H_2 and LPG sensor *Nanoscale* **7** 11971–9

[20] Nantao H *et al* 2014 Ultrafast and sensitive room temperature NH_3 gas sensors based on chemically reduced graphene oxide *Nanotechnology* **25** 025502

[21] Illyaskutty N, Kohler H, Trautmann T, Schwotzer M and Mahadevan Pillai V P 2013 Hydrogen and ethanol sensing properties of molybdenum oxide nanorods based thin films: effect of electrode metallization and humid ambience *Sensors Actuators* B **187** 611–21

[22] Boudiba A *et al* 2013 Sensitive and rapid hydrogen sensors based on Pd–WO_3 thick films with different morphologies *Int. J. Hydrog. Energy* **38** 2565–77

[23] Anand K, Singh O, Singh M P, Kaur J and Singh R C 2014 Hydrogen sensor based on graphene/ZnO nanocomposite *Sensors Actuators* B **195** 409–15

[24] Kumar R *et al* 2011 Fast response and recovery of hydrogen sensing in Pd–Pt nanoparticle–graphene composite layers *Nanotechnology* **22** 275719

[25] Phan D-T and Chung G-S 2014 Reliability of hydrogen sensing based on bimetallic Ni–Pd/graphene composites *Int. J. Hydrog. Energy* **39** 20294–304

[26] Zöpfl A, Lemberger M-M, König M, Ruhl G, Matysik F-M and Hirsch T 2014 Reduced graphene oxide and graphene composite materials for improved gas sensing at low temperature *Faraday Discuss.* **173** 403–14

[27] Russo P A *et al* 2012 Room-temperature hydrogen sensing with heteronanostructures based on reduced graphene oxide and tin oxide *Angew. Chem., Int. Ed.* **51** 11053–7

[28] Pandey P A, Wilson N R and Covington J 2013 Pd-doped reduced graphene oxide sensing films for H_2 detection *Sensors Actuators* B **183** 478–87

[29] Miremadi B K, Singh R C, Morrison S R and Colbow K 1996 A highly sensitive and selective hydrogen gas sensor from thick oriented films of MoS_2 *Appl. Phys.* A **63** 271–5

[30] Kanezashi M, Yamamoto A, Yoshioka T and Tsuru T 2010 Characteristics of ammonia permeation through porous silica membranes *AIChE J.* **56** 1204–12

[31] Kammeyer C W and Whitman D 1972 Quantum mechanical calculation of molecular radii: I. Hydrides of elements of periodic groups IV through VII *J. Chem. Phys.* **56** 4419–21

[32] You Y, Sahajwalla V, Yoshimura M and Joshi R K 2016 Graphene and graphene oxide for desalination *Nanoscale* **8** 117–9

[33] Amadei C A and Vecitis C D 2016 How to increase the signal-to-noise ratio of graphene oxide membrane research *J. Phys. Chem. Lett.* **7** 3791–7